

# Simulating Quantum Dynamics in the Manhattan Lattice

Addison Hartman

*2020 Physics REU, Department of Physics, University of California, Santa Barbara and  
Department of Physics and Department of Mathematics, Amherst College*

David Weld (Faculty Advisor)

*Department of Physics, University of California, Santa Barbara*

(Dated: Aug 21, 2020)

Bose-Einstein condensates have been an invaluable probe of quantum physics for the past two decades. However, questions about quantum chaos remain unanswered. Given the correspondence principle, we expect there to be some form of quantum chaos that approaches classical chaos as systems become macroscopic, but there is no consensus about how this quantum chaos would present itself. In this paper we propose a quantum analogue to a classically chaotic system—the bean machine—and develop a numeric simulation to predict the outcome of the experiment.

## I. INTRODUCTION

### A. Chaos

A classic example of chaos is a bean machine, illustrated in Fig. 1. At each level of pegs, a ball dropped into the machine goes either left or right, taking a random walk in 1D. Because a small change in initial condition drastically affects the system evolution, this exhibits classically chaotic behavior.

Given the correspondence principle, we expect there to be some form of “quantum chaos” that approaches classical chaos as we move into the classical regime. However, there is not yet consensus on what quantum chaos is or what signatures it would present in a system. In order to probe this question,<sup>1</sup> we will construct a quantum analogue to the classically chaotic system of a bean machine. Instead of having individual balls propagating through a pegboard, our quantum analogue will have a single quantum wave function.

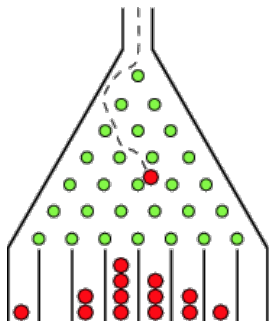


FIG. 1: A bean machine. Each bean takes a random walk through the pegs, demonstrating classical chaos. Figure from [1].

In order to construct our quantum bean machine and be able to observe its behavior, we require two things:

1. an imageable quantum wave function, and
2. a pegboard potential to confine our wave function.

A quick consideration of our first requirement does not bode well; quantum mechanics stipulates that if we image a quantum particle, its wave function collapses and we find it at a single position. We are interested in the dynamics of the quantum wave function itself, so this will not suffice. Perhaps we could run our experiment over and over, slowly constructing a statistical picture of the wave function at some time. Again, this would only give us one snapshot in time, and we would have to run our experiment many more times to create a dynamic model. Fortunately, there is a much better tool in the ultracold atomic physicist’s shed: the Bose-Einstein condensate.

### B. Bose-Einstein Condensates

Bose-Einstein condensates (BECs) are a phase of matter in which quantum phenomena become macroscopic because every particle has the same wave function. First realized in the laboratory in 1995 (an achievement which won the 2001 Nobel Prize), BECs are an incredibly useful tool in contemporary experiments as probes of quantum physics.

A BEC is a perfect candidate for our imageable quantum wave function. In the Weld Lab, we make strontium-84 BECs with approximately  $8 \times 10^4$  atoms.<sup>2</sup> Imaging the BEC causes each atom’s wave function to collapse, but since all of these particles occupy the same quantum state, they statistically distribute themselves according to the common wave function! Fig 2 shows three such images.

<sup>1</sup> We are also interested in the topics of boson sampling and matter wave interference, into which this system may provide insight.

<sup>2</sup> This number is consistent to  $\pm 10\%$ .

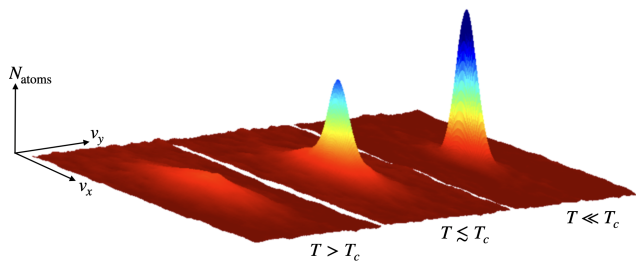


FIG. 2: Momentum-space image of a  $^{84}\text{Sr}$  BEC in the Weld Lab at UCSB. Temperature reaches the condensation temperature from left to right. Figure from [4].

In the lab, a BEC is made by optically cooling atoms<sup>3</sup> to temperatures on the order of 10 nK. At the condensation temperature  $T_c$  determined by the atom’s mass and the gas’s density,<sup>4</sup> the atoms condense abruptly into the single-particle ground momentum and position state, a discontinuous process which indicates a phase transition. In Fig. 2, this condensation process is clearly seen. While this behavior may be expected at absolute zero, the amazing thing about bosons is that they condense at a finite temperature.

In the Weld Lab at UCSB, a strontium-84 ( $^{84}\text{Sr}$ ) BEC is made in the “strontium machine” (Fig. 3) through a number of steps:<sup>5</sup>

0. atomic oven: heat strontium and collimate through a nozzle to form an atom beam
1. transverse cooling: laser cool perpendicular to direction of atom beam to further collimate
2. Zeeman slower: laser cool using a gradient magnetic field and Zeeman splitting to keep the relevant optical transition on resonance with the laser as the atoms slow down
3. blue magneto-optical trap (MOT): trap and laser cool, targeting a wide linewidth transition for fast cooling
4. stable magnetic trap: trap atoms while transitioning between blue and red MOTs
5. red MOT: trap and laser cool, targeting a narrow linewidth transition for reaching lower temperatures

<sup>3</sup> The atoms must be composite bosons. Fermions obey the Pauli exclusion principle and thus can never all occupy the single-particle ground state.

<sup>4</sup> For our  $^{84}\text{Sr}$  BEC with  $8 \times 10^4$  atoms,  $T_c \approx 150$  nK [2]. By the time the cooling process is over, the condensate temperature is  $< 100$  nK and the condensate fraction is nearly 1 [3].

<sup>5</sup> For more detailed explanations, see Appendix A.

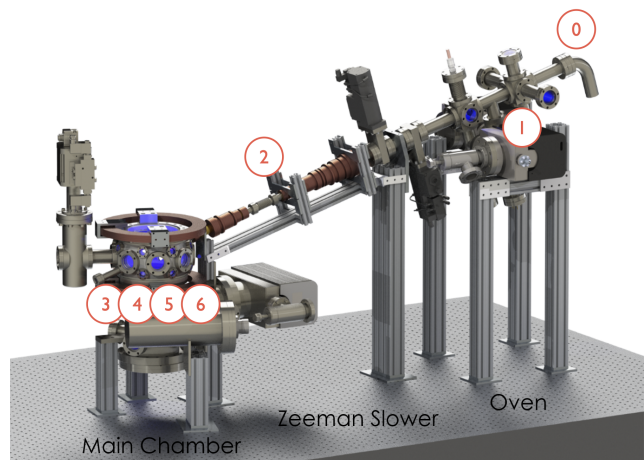


FIG. 3: Strontium BEC machine, with numbered cooling steps. Figure from [2].

6. forced evaporative cooling: decrease trap depth of optical dipole trap (ODT) to remove the warmest atoms, leaving the others to rethermalize and form a BEC

After we have made a BEC in the lab, we are free to run experiments on it within the main chamber, which is where the BEC is held.

### C. The Manhattan Lattice

The AC Stark shift allows certain configurations of lasers to create an optical potential for our BEC by inducing electric dipole moments in the strontium atoms. The beam machine is a 2D system, so we must develop a 2D potential with peg-like features through which we can propagate our BEC. A static 2D orthogonal beam lattice with phase-locked beams produces the potential [5]

$$\bar{V}(\bar{x}, \bar{y}) = \frac{1}{2}V_X \cos(2k_L\bar{x}) + \frac{1}{2}V_Y \cos(2k_L\bar{y}) + 2\sqrt{V_X V_Y} \cos(k_L\bar{x}) \cos(k_L\bar{y}), \quad (1)$$

where  $V_X$  and  $V_Y$  are the lattice depths in each dimension,  $k_L = 2\pi/\lambda$  is the wavenumber of the lasers, and the bars denote a dimensionalized version of a variable which will be nondimensionalized in §II B. If the two beams are equal in power ( $V_X = V_Y = V_0$ ), Eq. (1) becomes

$$\bar{V}(\bar{x}, \bar{y}) = \frac{1}{2}V_0 \cos(2k_L\bar{x}) + \frac{1}{2}V_0 \cos(2k_L\bar{y}) + 2V_0 \cos(k_L\bar{x}) \cos(k_L\bar{y}). \quad (2)$$

We call this potential, shown in Fig. 4, the “Manhattan lattice<sup>6</sup>” for the apparent streets of low potential and skyscrapers of high potential.

<sup>6</sup> Note that this potential is not a lattice in the usual sense of the word because it does hold atoms in local minima, or “lat-

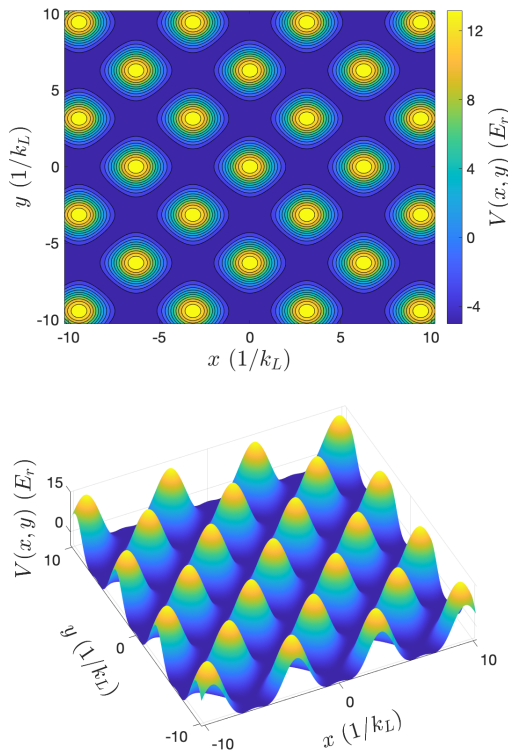


FIG. 4: The Manhattan potential.

Now that we have an imageable wave function in the form of a BEC and a pegboard in the form of the Manhattan lattice, we are ready to begin exploring the quantum dynamics of our system.

## II. METHODS

In addition to watching the physics unfold in the lab, it is important to understand the theory behind the physics and be able to replicate the dynamics we observe with simulations.<sup>7</sup> Ironically, the problem of boson sampling has been shown to be quantum-hard, so it is effectively impossible to analytically solve on a classical computer [6]. For this reason, a numerical approach is necessitated, which we do in the Matlab language.

\_\_\_\_\_

tice sites.” Despite this, we have chosen to use the familiar terminology because there is an intuitive connection between our potential and a typical optical lattice.

<sup>7</sup> The complications of COVID-19 only further motivated experimentalists to delve into the world of numerics. I, like many others, made this transition unwillingly, but grew to appreciate the deeper understanding simulations provide us. The rest of this report thus focuses on the numeric simulation of the quantum beam machine, not its experimental implementation.

### A. Discretizing Space and Time

A numerical approach requires a discrete grid of points to compute over. In Matlab, these are obtained by using the `meshgrid()` function<sup>8</sup> and are centered around zero. For computational efficiency, there are  $N = 2^n$  points in both the  $x$  and  $y$  dimensions, spaced by  $dx$ . The discrete Fourier transform allows us to go from a position-space representation to a representation in momentum, so naturally momentum space will be discretized as well with the same number of points in each dimension and spacing

$$dk_x = \frac{2\pi}{dx(N-1)}. \quad (3)$$

To discretize time, we simply choose a  $dt < 0.1$  in nondimensionalized units for accuracy. Because there are often thousands of time steps, we save the wave function at regular intervals rather than at every step. We can then analyze the dynamics of these saved wave functions for signatures of quantum chaos.

### B. Non-dimensionalizing the Hamiltonian

In 2D with dimensionalized units, the Hamiltonian is

$$\hat{H} = -\frac{\hbar^2}{2m}\bar{\nabla}^2 + \bar{V}(\bar{x}, \bar{y}), \quad (4)$$

where  $\hbar$  is the reduced Planck’s constant,  $m$  is the mass of the particle, and the Laplacian is

$$\bar{\nabla}^2 = \frac{\partial^2}{\partial \bar{x}^2} + \frac{\partial^2}{\partial \bar{y}^2}. \quad (5)$$

However, the constants in this equation tend to have very small values, and there is a risk of losing accuracy in computer simulations due to how computers store numbers. For this reason, we wish to “non-dimensionalize” the Hamiltonian.<sup>9</sup> First, we determine the characteristic length and energy scales of our system,

$$L_s = \frac{1}{k_L} \quad E_s = E_r, \quad (6)$$

where  $E_r$  is the recoil energy of absorbing a photon,

$$E_r = \frac{\hbar^2 k_L^2}{2m}. \quad (7)$$

With these scales, we can define dimensionless quantities sans bars over the top:

$$x = k_L \bar{x} \quad y = k_L \bar{y} \quad (8)$$

$$V = \frac{\bar{V}}{E_r} \quad \hat{H} = \frac{\hat{H}}{E_r}. \quad (9)$$

\_\_\_\_\_

<sup>8</sup> See Appx. B1 for details.

<sup>9</sup> This also makes the numerical results applicable to any atom.

By substituting for these values in Eqs. (2) and (4), we obtain the dimensionless equations

$$\begin{aligned}\bar{V}(x, y) &= \frac{1}{2}V_0 E_r \cos(2x) + \frac{1}{2}V_0 E_r \cos(2y) \\ &\quad + 2V_0 E_r \cos(x) \cos(y) \\ V(x, y) &= \frac{1}{2}V_0 \cos(2x) + \frac{1}{2}V_0 \cos(2y) \\ &\quad + 2V_0 \cos(x) \cos(y)\end{aligned}\quad (10)$$

and

$$\begin{aligned}\hat{H} &= -\frac{1}{E_r} \frac{\hbar^2}{2m} \bar{\nabla}^2 + \frac{\bar{V}(x, y)}{E_r} \\ &= -k_L^2 \bar{\nabla}^2 + V(x, y) \\ \hat{H} &= -\nabla^2 + V(x, y).\end{aligned}\quad (11)$$

We also have a characteristic time scale for the system,

$$T_s = \frac{1}{\omega_r},$$

where  $\omega_r$  is the recoil frequency

$$\omega_r = \frac{E_r}{\hbar} = \frac{\hbar k_L^2}{2m}.$$

Our time evolution uses discretized time steps in these units.

### C. Time Evolution

The time evolution operator for some infinitesimal time  $dt$  is  $e^{-i\hat{H}dt}$ .<sup>10</sup> Ideally, we would like to apply this operator to our wave function to step it forward a time  $dt$ :

$$\Psi(\mathbf{x}, t + dt) = e^{-i\hat{H}dt} \Psi(\mathbf{x}, t). \quad (12)$$

However, there is not a clear way to write the Hamiltonian as a diagonalized matrix for a non-static potential, so the exponent is too hard of a calculation. Instead, we note that the (nondimensionalized) time-dependent Schrödinger equation,

$$i \frac{\partial}{\partial t} \Psi(\mathbf{x}, t) = \hat{H} \Psi(\mathbf{x}, t) = (-\nabla^2 + V(\mathbf{x}, t)) \Psi(\mathbf{x}, t), \quad (13)$$

is in the form

$$\frac{\partial}{\partial t} u = Au + Bu. \quad (14)$$

For equations of this type, the approximation

$$e^{(A+B)dt} \approx e^{Adt} e^{Bdt} \quad (15)$$

<sup>10</sup> Up to a factor of  $\hbar$ , which is identified with unity by nondimensionalizing our units.

can be made.<sup>11</sup> In our case,

$$A = i\nabla^2 \quad B = -iV(\mathbf{x}, t). \quad (16)$$

Thus the position and momentum portions of the time evolution operator, which we call *propagators*, can be applied separately to the wave function. Because these propagators are supposed to be applied at the same time, an even better approximation is

$$e^{(A+B)dt} \approx e^{\frac{Bdt}{2}} e^{Adt} e^{\frac{Bdt}{2}}. \quad (17)$$

There is still a problem with this plan: it is not ideal to apply  $e^{i\nabla^2 dt}$  to the wave function in position space  $\Psi(\mathbf{x}, t)$  because (1)  $\nabla$  is not a diagonal operator in the position basis, which makes the matrix calculation computationally costly, and (2) derivatives on a discretized space must be approximated. For these reasons, we transform both the wave function and momentum propagator to the momentum basis:<sup>12</sup>

$$\Psi(\mathbf{x}, t) \rightarrow \Phi(\mathbf{k}, t) \quad (18)$$

$$e^{i\nabla^2 dt} \rightarrow e^{-i\mathbf{k}^2 dt}. \quad (19)$$

Thus our propagators are

$$U_k = e^{-i\mathbf{k}^2 dt} \quad U_V = e^{-iV(\mathbf{x}, t)dt/2}. \quad (20)$$

We step forward a time  $dt$  by multiplying by the propagators, transforming between bases in between with the discrete Fourier transform  $\mathcal{F}$  and inverse discrete Fourier transform  $\mathcal{F}^{-1}$ :

$$\Psi(\mathbf{x}, t + dt) = U_V \left[ \mathcal{F}^{-1} \left( U_k \left[ \mathcal{F} \left( U_V \left[ \Psi(\mathbf{x}, t) \right] \right) \right] \right) \right]. \quad (21)$$

In its entirety, this method of numerical time propagation is called the *time-splitting spectral method*, or TSSP.<sup>13</sup> Importantly, TSSP is also applicable to nonlinear Schrödinger equations such as the Gross-Pitaevskii equation mentioned in §V.

## III. SIMULATION PROCEDURE

### A. Initial State

Our simulation must begin with the same wave function produced by the crossed optical dipole trap (ODT) potential in the strontium machine. Ignoring interactions

<sup>11</sup> In general, for matrices  $A$  and  $B$ ,  $e^{A+B} = e^A e^B$  if and only if  $[A, B] = 0$ , that is, if and only if they commute.

<sup>12</sup> For details about the extra complications of the basis transformation process in Matlab, see Appx. B 2.

<sup>13</sup> Confusingly, these letters don't exactly match what they are abbreviating. Additionally, TSSP can stand for the time-splitting sine-spectral, pseudospectral, or sine-pseudospectral methods as well.

between particles in the BEC,<sup>14</sup> this potential is modelled well by a harmonic oscillator potential and as such, the initial state of the BEC after condensation is the ground state of a 2D harmonic oscillator [7],

$$\frac{1}{\sqrt{\pi a_x a_y}} \exp\left(-\frac{1}{2}\left(\frac{x^2}{a_x^2} + \frac{y^2}{a_y^2}\right)\right), \quad (22)$$

where the oscillator lengths are

$$a_i = \sqrt{\frac{\hbar}{m\omega_i}} k_L \quad (23)$$

in dimensionless units of  $L_s$  from Eq. (6). In our experiment, the trap frequencies in the  $x$  and  $y$  dimensions are  $\omega_x = 270$  Hz and  $\omega_y = 430$  Hz<sup>15</sup> [2]. These are significantly different frequencies, so we can safely assume that these beams do not interfere with each other (or the lattice beams), and the potential given by both lasers is the sum of their individual potentials.

### B. Ramp and Free Evolution

There are two phases to the time evolution: ramp and free evolution. While we could simply set the initial wave function free on top of the lattice potential, this wave function has very high energy components not representative of a beam machine. Instead, we consider a lower energy state by “ramping” up the lattice potential on top of the ODT potential adiabatically from  $t = 0$  to  $t_{\text{ramp}}$ , a process taking around 100 ms. The ODT potential for a harmonic oscillator is

$$\bar{V}_{\text{ODT}} = \frac{1}{2}m(\omega_x^2 \bar{x}^2 + \omega_y^2 \bar{y}^2). \quad (24)$$

As before, our  $x$  and  $y$  are unitless, so we multiply by the square of the characteristic length scale  $L_s = 1/k_L$  to recover  $\bar{V}_{\text{ODT}}$  in the proper units of joules:

$$\bar{V}_{\text{ODT}} = \frac{m}{2k_L^2}(\omega_x^2 x^2 + \omega_y^2 y^2). \quad (25)$$

To make the potential unitless, we divide by the characteristic energy scale  $E_s = E_r$  and obtain

$$V_{\text{ODT}} = \frac{m}{2E_r k_L^2}(\omega_x^2 x^2 + \omega_y^2 y^2). \quad (26)$$

To make the effect of a tilted lattice similar to the tilt of a beam machine, we add a gravitational potential which can be adjusted for different tilts:

$$V_{\text{grav}} = -F_X x - F_Y y. \quad (27)$$

During the ramp period, the Hamiltonian uses the combined ramp potential,

$$V_{\text{ramp}} = V_{\text{ODT}} + \frac{t}{t_{\text{ramp}}}(V_{\text{lat}} + V_{\text{grav}}), \quad (28)$$

and after the ramp period, we snap off the ODT potential such that

$$V_{\text{free}} = V_{\text{lat}} + V_{\text{grav}} \quad (29)$$

and allow the wave function to freely evolve until a time  $t_f$ .

## IV. RESULTS

We have developed a tool to simulate the quantum dynamics of a BEC in the Manhattan lattice. We can vary experimental parameters such as BEC size, lattice depth, lattice tilt, ramp time, and end time. We can also vary parameters of the simulation such as position and momentum mesh size, time step size, and how often we store the wave function for analysis.

Our code provides a few different ways to analyze each simulation. First, each simulation produces a gif of the probability density  $|\Psi(\mathbf{x}, t)|^2$  using the saved position-basis wave functions. A few frames from a sample gif are shown in Fig. 5.

It is also important to have results from each simulation which are directly comparable to measurements we can make in the lab of a BEC. One of these measurements is a time-of-flight measurement where the BEC is instantaneously released from all optical potentials and free-expands, effectively transforming the atom cloud into momentum space. A picture can then be taken of the BEC. To obtain directly comparable images from our simulation, we can Fourier transform the saved position-basis wave functions to create a series of momentum space pictures.

The code and documents relating to this project can be found at [https://github.com/weldlabucsb/Manhattan\\_lattice](https://github.com/weldlabucsb/Manhattan_lattice).

## V. FURTHER WORK

The next expansion on our simulations will include interactions between particles. The nondimensionalized time-dependent Gross-Pitaevski equation (GPE) [7],

$$i \frac{\partial}{\partial t} \Psi(\mathbf{x}, t) = -\nabla^2 + V(\mathbf{x}, t) + g|\Psi(\mathbf{x}, t)|^2, \quad (30)$$

includes an interaction term  $g$  which accounts for inter-particle interactions. In three dimensions, we know

$$g = \frac{4\pi\hbar^2 a_s}{m},$$

<sup>14</sup> A BEC is better modelled as having weakly interacting bosons, for which the ground state is a Thomas-Fermi profile [3]. This is discussed in §V.

<sup>15</sup> The trap frequency of an ODT can be measured by driving the trap at a range of frequencies until a resonant excitation is seen in the BEC.

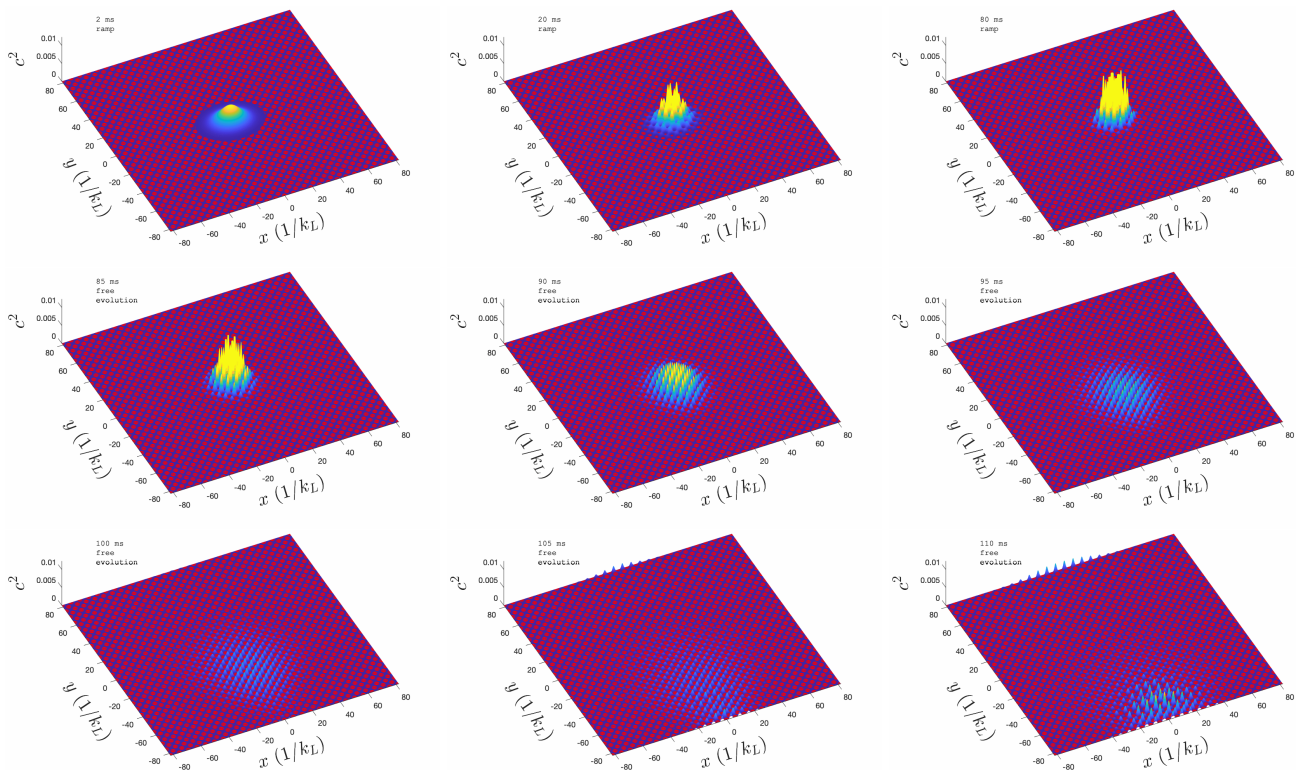


FIG. 5: Frames from a sample evolution gif. The absolute square of the wave function is overlain with red contours of the Manhattan potential. The first row shows the ramp stage at 2, 20, and 80 ms, while the bottom two rows show the free evolution phase in increments of 5 ms. Border effects are noticeable in the last two frames.

where  $a_s$  is the s-wave scattering length.<sup>16</sup> In two dimensions, however, it is less obvious what  $g$  should be.

Using the GPE complicates our calculations in a few other ways as well. First, the ground state of a BEC obeying the GPE in a harmonic trap is a Thomas-Fermi distribution, not the ground state of a simple harmonic oscillator [7]. Second, the position propagator  $U_V$  defined in Eq. (20) will become time-dependent and thus will have to be re-calculated at each time step in the propagation, as follows [8]:

$$U_V = \exp\left(-\frac{i}{2} \left[ V(\mathbf{x}, t) + g|\Psi(\mathbf{x}, t)|^2 \right]^2 dt\right). \quad (31)$$

We also plan to construct a laser system for the Manhattan lattice and run experiments with our strontium BEC, which can then be compared to the simulations and analyzed for signatures of quantum chaos.

## VI. ACKNOWLEDGEMENTS

I would like to thank my advisor, David Weld, for transforming my REU project into something which could be done virtually and providing motivation and insights throughout. My graduate mentor, Peter Dotti, was invaluable to me this summer as my go-to person for answering questions from physics to Matlab to the computer cluster to graduate school. I would also like to thank Jared Pagett for being open to questions about dipole traps and lattices and everyone else in the Weld Lab for welcoming me into their virtual lab meetings and message channels, providing a sense of community despite the distance. Lastly, thank you to Sathya Guruswamy, the director of the UCSB REU program, for coordinating a number of events and providing advice and motivation throughout the summer. This work was supported by NSF REU grant PHY-1852574. Additionally, use was made of the computational facilities administered by the Center for Scientific Computing at the CNSI and MRL (an NSF MRSEC; DMR-1720256) and purchased through NSF CNS-1725797.

<sup>16</sup> For  $^{84}\text{Sr}$ ,  $a_s = 123a_0$ , where  $a_0$  is the Bohr radius. This is a convenient length for evaporative cooling, and why we use the  $^{84}\text{Sr}$  isotope despite its low abundance [3].

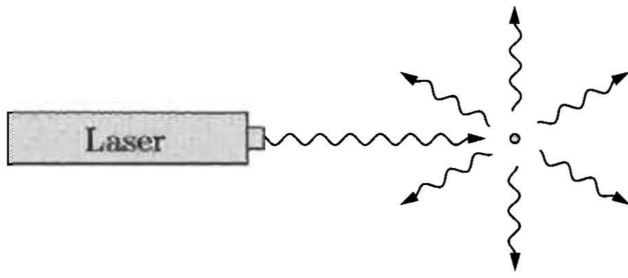


FIG. 6: Laser cooling. Figure from [9].

## Appendix A: Cooling Phases

### 1. Laser cooling

Due to the fact that photons carry momentum, when an atom absorbs a photon, it loses the momentum of the photon  $p = h/\lambda$  in the direction from which the photon came. Excited energy levels are often unstable, and thus the atom will re-emit a photon some time later. This photon, emitted in a random direction, also carries momentum and thus “pushes” the atom as it leaves. However, if we use a directional source for the absorbed photons as shown in Fig. 6, there will be a net loss of momentum for the atom in the direction of the laser, and the atom will be cooled in that direction.

Atoms in a beam, such as in steps 1 or 2 of Fig. 3, can be further collimated by lasers perpendicular to their direction of travel and slowed by counterpropagating lasers.

### 2. Zeeman slowers

As an atom beam travels along the axis of a Zeeman slower, they are slowed by laser cooling, shifting the target transition out of resonance with the laser. To compensate, a gradient magnetic field continuously varies the target optical transition via the Zeeman effect to maintain resonance with the cooling laser at the expected rate of slowing.

### 3. Magneto-optical traps

Magneto-optical traps (MOTs) consist of two anti-Helmholtz coils and three pairs of counter-propagating beams, as shown in Fig. 7. The magnet coils provide a linearly varying magnetic field that shifts the optical transition targeted by the lasers into resonance when an atom is moving *away* from the center of the trap. This applies a force on that atom *towards* the center of the trap, which simultaneously cools and traps the cloud of atoms.

The blue MOT uses a wide linewidth (461 nm) transition for rapid cooling, while the red MOT uses a narrow (689 nm) transition for reaching lower temperatures.

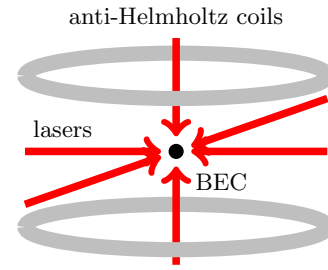


FIG. 7: Magneto-optical trap.

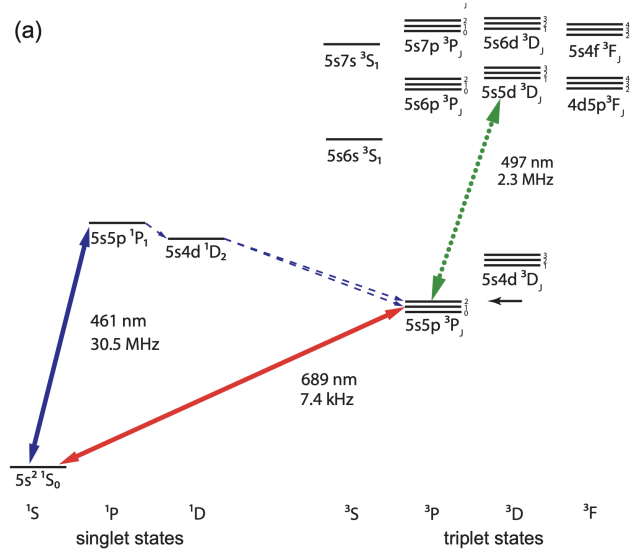


FIG. 8: Energy levels of strontium. The 461 nm transition is used for the blue MOT and the 689 nm transition is used for the red MOT. Figure from [10].

Fig. 8 shows the level structure of strontium with the relevant optical transitions labelled.

## Appendix B: MATLAB

### 1. meshgrid()

For the numerical approach in Matlab, we do not have exact functions for the wave function and each potential which are analytically calculated. Instead, we have a “mesh” of points in a 2D grid at which each of these “functions” are evaluated. An example position mesh is made below:

```

1 % number of points in a power of 2
2 Nx      = 4;
3 Ny      = 8;
4
5 % position mesh spacing in 1/kL
6 dx      = 1;
7 dy      = 1;
8
9 % position mesh points

```

```

10 xVals = dx*(-Nx/2:1:Nx/2-1);
11 yVals = dy*(-Ny/2:1:Ny/2-1);
12
13 % position mesh
14 [X,Y] = meshgrid(xVals,yVals);

```

The number of points affects computational efficiency<sup>17</sup> and  $dx$  and  $dy$  affect the accuracy of the simulation, so we generally explicitly pick both these values instead of substituting one for the  $x$  and  $y$  range. The above code, when run, creates the following  $8 \times 4$  matrices:

$$X = \begin{bmatrix} -2 & -1 & 0 & 1 \\ -2 & -1 & 0 & 1 \\ -2 & -1 & 0 & 1 \\ -2 & -1 & 0 & 1 \\ -2 & -1 & 0 & 1 \\ -2 & -1 & 0 & 1 \\ -2 & -1 & 0 & 1 \\ -2 & -1 & 0 & 1 \end{bmatrix} \quad Y = \begin{bmatrix} -4 & -4 & -4 & -4 \\ -3 & -3 & -3 & -3 \\ -2 & -2 & -2 & -2 \\ -1 & -1 & -1 & -1 \\ 0 & 0 & 0 & 0 \\ 1 & 1 & 1 & 1 \\ 2 & 2 & 2 & 2 \\ 3 & 3 & 3 & 3 \end{bmatrix} \quad (\text{B1})$$

There are a couple important things to notice about these matrices:

- There are two matrices, not one. This allows you to use  $X$  and  $Y$  in functions similarly<sup>18</sup> to how you would typically use  $x$  and  $y$  variables.

- The `meshgrid()` function takes arguments in the order  $(x,y)$ , where  $x$  describes columns and  $y$  describes rows, as opposed to the traditional  $(i,j)$  indices for (row, column) pairs in matrices.

Additionally, you may notice that zero is not centered in these matrices. While never inherently bad for the simulation, it becomes negligible when the number of points is on the order of  $2^{16}$  in each dimension.

## 2. `fft2()`, `ifft2()`, and `fftshift()`

To shift from the position to the momentum base as described in §II C, we utilize Matlab's built-in 2D fast Fourier transform, `fft2()` and corresponding inverse function, `ifft2()`, to transform back. A critical fact is that in Matlab, the  $x$  and  $y$  values are shifted by  $N_x/2$  and  $N_y/2$  in the `fft2()` function, respectively. This means the  $(1,1)$  entry in the transformed matrix corresponds to the first positive  $x$  and  $y$  values.  $x$  and  $y$  then increase as you move right or down, respectively, until they reach their maximum values  $(x_{N_x/2-1}, y_{N_y/2-1})$  at the center of the matrix. Then the elements jump back to the minimum values  $(x_{-N_x/2}, y_{-N_y/2})$  and increase to  $(x_{-1}, y_{-1})$  in the lower right-hand corner of the matrix. The full matrix maps as shown:

$$c(x, y) = \begin{bmatrix} c(x_{-N_x/2}, y_{-N_y/2}) & \dots & c(x_0, y_{-N_y/2}) & \dots & c(x_{N_x/2-1}, y_{-N_y/2}) \\ \vdots & \ddots & \vdots & \ddots & \vdots \\ c(x_{-N_x/2}, y_0) & \dots & c(x_0, y_0) & \dots & c(x_{N_x/2-1}, y_0) \\ \vdots & \ddots & \vdots & \ddots & \vdots \\ c(x_{-N_x/2}, y_{N_y/2-1}) & \dots & c(x_0, y_{N_y/2-1}) & \dots & c(x_{N_x/2-1}, y_{N_y/2-1}) \end{bmatrix} \quad (\text{B2})$$

$$\hat{c}(k_x, k_y) = \begin{bmatrix} \hat{c}(k_{x_0}, k_{y_0}) & \dots & \hat{c}(k_{x_{N_x/2-1}}, k_{y_0}) & \hat{c}(k_{x_{-N_x/2}}, k_{y_0}) & \dots & \hat{c}(k_{x_{-1}}, k_{y_0}) \\ \vdots & \ddots & \vdots & \vdots & \ddots & \vdots \\ \hat{c}(k_{x_0}, k_{y_{N_y/2-1}}) & \dots & \hat{c}(k_{x_{N_x/2-1}}, k_{y_{N_y/2-1}}) & \hat{c}(k_{x_{-N_x/2}}, k_{y_{N_y/2-1}}) & \dots & \hat{c}(k_{x_{-1}}, k_{y_{N_y/2-1}}) \\ \hat{c}(k_{x_0}, k_{y_{-N_y/2}}) & \dots & \hat{c}(k_{x_{N_x/2-1}}, k_{y_{-N_y/2}}) & \hat{c}(k_{x_{-N_x/2}}, k_{y_{-N_y/2}}) & \dots & \hat{c}(k_{x_{-1}}, k_{y_{-N_y/2}}) \\ \vdots & \ddots & \vdots & \vdots & \ddots & \vdots \\ \hat{c}(k_{x_0}, k_{y_{-1}}) & \dots & \hat{c}(k_{x_{N_x/2-1}}, k_{y_{-1}}) & \hat{c}(k_{x_{-N_x/2}}, k_{y_{-1}}) & \dots & \hat{c}(k_{x_{-1}}, k_{y_{-1}}) \end{bmatrix}, \quad (\text{B3})$$

where the indices for  $x, y, k_x$ , and  $k_y$ , as described in Appx. B1, range from  $-N_i/2$  to  $N_i/2 - 1$  and have values of  $dx, dy, dk_x$ , or  $dk_y$  times their index, respectively. To obtain the desired momentum-space matrix,

$$\hat{c}'(k_x, k_y) = \begin{bmatrix} \hat{c}(k_{x_{-N_x/2}}, k_{y_{-N_y/2}}) & \dots & \hat{c}(k_{x_0}, k_{y_{-N_y/2}}) & \dots & \hat{c}(k_{x_{N_x/2-1}}, k_{y_{-N_y/2}}) \\ \vdots & \ddots & \vdots & \ddots & \vdots \\ \hat{c}(k_{x_{-N_x/2}}, k_{y_0}) & \dots & \hat{c}(k_{x_0}, k_{y_0}) & \dots & \hat{c}(k_{x_{N_x/2-1}}, k_{y_0}) \\ \vdots & \ddots & \vdots & \ddots & \vdots \\ \hat{c}(k_{x_{-N_x/2}}, k_{y_{N_y/2-1}}) & \dots & \hat{c}(k_{x_0}, k_{y_{N_y/2-1}}) & \dots & \hat{c}(k_{x_{N_x/2-1}}, k_{y_{N_y/2-1}}) \end{bmatrix}, \quad (\text{B4})$$

<sup>17</sup> We are actually primarily limited by memory space, as these matrices easily take tens of gigabytes. When editing code, reduce  $N$  and run trials locally. For larger simulations, a computer

cluster is necessary.

<sup>18</sup> To maintain element-wise operations instead of the default matrix operations, use a period before each operator (e.g. “.\*” as opposed to “\*”).

we could use the `fftshift()` function. In practice, it is computationally faster to apply `fftshift()` to our momentum propagator defined in Eq. (20), so the actual time propagation, broken into individual steps, is as follows:

```

1 c = UV.*c;           % propagate in position
2 c = fft2(c);        % transform to momentum space
3 c = fftshift(Uk).*c; % propagate in momentum
4 c = ifft2(c);       % transform to position space
5 c = UV.*c;         % propagate in position

```

- 
- [1] Wolfram mathworld, galton board, <https://mathworld.wolfram.com/GaltonBoard.html>.
  - [2] S. Rajagopal, *Realizing and probing driven quantum systems with ultracold gases*, Ph.D. thesis, University of California, Santa Barbara (2019).
  - [3] R. Senaratne, *Quantum Simulation of Strongly-Driven Systems Using Ultracold Lithium and Strontium*, Ph.D. thesis, University of California, Santa Barbara (2018).
  - [4] D. Weld, Weld lab, <http://web.physics.ucsb.edu/~weld/>.
  - [5] P. Dotti, N interfering lattice beams (2020), unpublished.
  - [6] S. Aaronson and A. Arkhipov, The computational complexity of linear optics (2010), arXiv:1011.3245 [quant-ph].
  - [7] C. J. Pethick and H. Smith, *Bose-Einstein Condensation in Dilute Gases*, 2nd ed. (Cambridge University Press, 2008).
  - [8] A. Cao, Weld lab primer on TDSE/GPE integration, unpublished.
  - [9] D. V. Schroeder, *An Introduction to Thermal Physics* (Addison Wesley Longman, 2000).
  - [10] S. Stellmer, *Degenerate quantum gases of strontium*, Ph.D. thesis, University of Innsbruck (2013).